sciendo

POLISH MARITIME RESEARCH 3 (119) 2023 Vol. 30; pp. 96-110
10.2478/pomr-2023-0043

FAULT DIAGNOSIS OF ME MARINE DIESEL ENGINE FUEL INJECTOR WITH NOVEL IRCMDE METHOD

Qingguo Shi *
Yihuai Hu
Guohua Yan
Shanghai Maritime University, Shanghai, China

* Corresponding author: *892158956@qq.com (Qingguo Shi)*

ABSTRACT

As an important component of the fuel injection system, the fuel injector is crucial for ensuring the power, economy, and emissions for a whole ME (machine electronically-controlled) marine diesel engine. However, injectors are most prone to failures such as reduced pressure at the opening valve, clogged spray holes and worn needle valves, because of the harsh working conditions. The failure characteristics are non-stationary and non-linear. Therefore, to efficiently extract fault features, an improved refined composite multi-scale dispersion entropy (IRCMDE) is proposed, which uses the energy distribution of sampling points as weights for coarse-grained calculation, then fast correlation-based filter(FCBF) and support vector machine (SVM) are used for feature selection and fault classification, respectively. The experimental results from a MAN B&W 6S35ME-B9 marine diesel engine show that the proposed algorithm can achieve 92.12% fault accuracy for injector faults, which is higher than multiscale dispersion entropy (MDE), refined composite multiscale dispersion entropy (RCMDE) and multiscale permutation entropy (MPE). Moreover, the experiment has also proved that, due to the double-walled structure of the high-pressure fuel pipe, the fuel injection pressure signal is more accurate than the vibration signal in reflecting the injector operating conditions.

Keywords: marine diesel engine; fuel injector; improved refined composite multi-scale dispersion entropy; fault diagnosis

INTRODUCTION

A diesel engine has the advantages of high reliability, high fuel economy and easy operations; it has been the main propulsion source for marine ships [1]. For a diesel engine, the fuel injection system is one of most important parts, its safe and reliable operation is crucial to ensuring the power, economy, and reliability of the whole engine [2]. With the development of technology and more stringent emission regulations, high pressure common rail fuel injection systems have become a hot research topic because of their good performance, in terms of power, economy and emissions [3]. The MAN B&W ME-type diesel engine has the largest scale of application of all marine two-stroke diesel engines. However, injector failure occurs at a higher rate, affecting the energy efficiency and emission performance of diesel engines [4]. Therefore, fault diagnosis in diesel fuel injectors is crucial to ensure the safe and efficient operation of marine diesel engines.

For the process of fault diagnosis, there are mainly three steps: signal acquisition, feature extraction, and pattern classification. Many researches have conducted fault diagnosis of diesel engines. Thurson et al. [5] measured the exhaust temperature to diagnose faults in diesel engine fuel injectors. Li et al. [6] analysed the cylinder pressure to reflect the whole

combustion process and identify the malfunctions of diesel engines. Zhang et al. [7] used the instantaneous crankshaft speed to realise the fault diagnosis of uneven firing intervals of V-type marine diesel engines. Yang et al. [8] collected vibration signals by installing a transducer on a fuel injection pump, and then used discriminative non-negative matrix factorisation and KNN classifier to realise the fault diagnosis of diesel engines. Ftoutou et al.[9] measured vibration signals on the cylinder block and used modified S-transform, two-dimensional non-negative matrix factorisation, and three fuzzy clustering algorithms to realise the fault diagnosis of a diesel engine's injection faults. Ramteke et al. [10] used signal processing techniques to extract fault-related features from vibration signals, and then monitored the effect of liner scuffing faults. Alireza et al. [11] presented a condition monitoring and combustion fault detection method based on the vibration signal obtained from both intake manifold and cylinder heads. Although vibration signals are easy to measure, they are more susceptible to contamination, especially under weak faults. For a marine two-stoke diesel engine, the vibration on a ship is inherently serious, so the vibration signals measured from the surface of diesel engines may not be accurate for fault diagnosis. Similarly for the fuel injection system, the fuel injection pipeline is relatively thick and may be a double-walled pipe, which makes it difficult to measure the vibration signal on the surface of the pipeline to reflect the pressure fluctuation inside the pipeline. Therefore, in order to obtain better fault diagnosis accuracy, our research measures the fuel pressure and vibration signals of the high-pressure fuel line at the same time, and compares the two signals for analysis.

When acquiring the original fluctuation signal, the next step is feature extraction. Many methods had been used to extract the fault features, mainly including time-domain analysis [12], frequency-domain analysis [13], and time-frequency analysis [14]. Because the pressure and vibration signals of high pressure pipes have nonlinear and non-stationary characteristics, nonlinear dynamic-based entropy methods are a powerful tool for extracting these features and they have been widely used in the field of fault diagnosis, e.g. approximate entropy (AE), sample entropy (SE), fuzzy entropy (FE), and permutation entropy (PE). Chen et al. [15] used SE for rolling bearing fault diagnosis. Shang et al. [16] used modified SE for the fault diagnosis of lithium-ion battery strings. Zhu et al. [17] used the FE to extract fault features. Ma et al. [18] used fuzzy distribution entropy for fault diagnosis in rotating machinery. However, these methods made comparisons between data, which may have reduced the calculation efficiency. Ma et al. [19] used PE for the early fault diagnosis of rotating machinery. Wu et al. [20] used multi-scale permutation entropy (MPE) for the fault diagnosis of bearings. However, PE values are relatively sensitive to noise [21]. In order to extract fault features more efficiently, Azami et al. [22] proposed dispersion entropy (DE). Gu et al. [23] used DE to realise the misfiring diagnosis of diesel engines. Yan et al. [24] used multi-scale dispersion entropy (MDE) to extract multidimensional fault characteristics and validated their effectiveness by experiments. Ke et al. [25] used hierarchical fluctuation dispersion entropy for fault diagnosis in common-rail injectors. Dhandapani et al. [26] used a generalised Gaussian distribution to refine composite multiscale dispersion entropy for the diagnosis of rolling bearings. Inspired by these references, we decided to use MDE to extract fault features from the pressure signal. However, the coarse-graining process in MDE has two main defects. Firstly, when the scale factor increases, the data length is reduced, and this reduces the reliability of the entropy value. Secondly, there are no overlap segments, and calculating the average of each segment will cause the loss of potentially useful information [27]. The coarse-graining process of refined composite MDE can solve these problems, to some extent, but it only considers the first-order moment in the coarse-graining process. Therefore, in this research, we propose an improved refined composite MDE (IRCMDE) to extract more hidden features for fault diagnosis, in which the second-order moment is used. After using IRCMDE, the fault features of the pressure signal can be extracted. However, these fault features are large and so feature reduction is needed for the improvement of calculation efficiency. Generally speaking, distance measures, dependency measures, consistency measures and information measures are used to evaluate the quality of a feature [28]; mutual information is most frequently used to measure the correlation and redundancy of features. The fast correlation-based filter (FCBF) has faster calculation efficiency and robustness, compared to the relevance filter, minimum redundancy maximum relevance (mRMR) and conditional mutual information maximisation (CMIM). Therefore, this study uses FCBF for feature selection and then constructs the feature set. After feature extraction and selection, state classification is the final step in fault diagnosis. Support vector machine (SVM) is one of the most commonly used fault classification methods, showing great advantages when fault sample data is insufficient. Zhang et al. [29] proposed the support vector machine (SVM)-based intelligent fault diagnosis method and obtained good results under different fault degrees at various engine speeds and load conditions. Zhao et al. [30] proposed PSO-SVM, to realise the fault classification. SVM is selected in this research, to classify the fault mode. Simulations and experiments were conducted to illustrate the diagnosis performance and generalisation ability of the proposed method.

The rest of this paper is organised as follows: in Section 2, theoretical analysis of IRCMDE is introduced. In Section 3, the influence of parameter changes on the IRCMDE value is discussed in detail and the effectiveness of the algorithm is demonstrated through simulation signals. In Section 4, the whole fault diagnosis procedure is proposed. In Section 5, experiments are employed to verify the proposed method. The conclusion is summarised in Section 6.

IMPROVED REFINED COMPOSITE MULTISCALE DISPERSION ENTROPY

For the original time series with N points, the length of the coarse-grained time series at scale factor τ is equal to N/τ after using the MDE method, as shown in Eq. (1). So, when a larger scale factor is used, the generated time series will become shorter. Besides, MDE divides the time series into non-overlapping segments of equal length and then calculates the average of all data points in each segment, which will inevitably cause the loss of potentially useful information. So, RCMDE is proposed to overcome the above defects; there two main steps to calculate the RCMDE value.

$$y_j^{\tau} = \frac{1}{\tau} \sum_{i=(j-1)\tau+1}^{j} x_i, 1 \le j \le N/\tau \tag{1}$$

Step 1. For a given time series u with length N, its k-th coarse-grained time sequence $y_k^{(\tau)} = \{y_{k,1}^{(\tau)}, y_{k,2}^{(\tau)}, \cdots, y_{k,\frac{N}{\tau}}^{(\tau)}\}$ can be calculated by Eq. (2).

$$\begin{aligned} y_{k,j}^{(\tau)} &= \frac{1}{\tau} \sum_{i=k+\tau(j-1)}^{k+j\tau-1} u_i \\ k &= 1,2,\cdots,\tau \\ j &= 1,2,\cdots,\frac{N}{\tau} \end{aligned} \tag{2}$$

Step 2. For each scale τ, the DE of each coarse-grained time series $y_k^{(\tau)}(k=1,2,\cdots,\tau)$ is calculated (the detailed calculation can be found in [23]). Then these DE values are averaged according to Eq. (3).

$$RCMDE(x,m,c,d,\tau) = \frac{1}{\tau}\sum_{k=1}^{\tau} DE(y_k^{(\tau)},m,c,d) \tag{3}$$

However, the RCMDE algorithm still uses the original coarse-grained mean processing, which affects the accuracy of entropy values. Inspired by this, the energy distributions between sampling points ($x_1, x_2, ..., x_n$) are used as coefficients to fuse the corresponding time scale factors $y_k^{(\tau)}$ and preserve the impact characteristics of the original signal to the greatest extent possible. The calculation flowchart of IRCMDE is shown in Fig.1. For the IRCMDE method, there are two main steps to calculate the IRCMDE value.

Step 1. For a given time series u with length N, its k-th coarse-grained time sequence $y_k^{(\tau)} = \{y_{k,1}^{(\tau)}, y_{k,2}^{(\tau)}, \cdots, y_{k,\frac{N}{\tau}}^{(\tau)}\}$ can be calculated by Eq. (4).

$$\begin{aligned} y_{k,j}^{\tau} &= \sum_{i=(j-1)\tau+k}^{j\tau+k-1} (x_i - \bar{x})^2 \Big/ \sum_{i=(j-1)\tau+k}^{js+k-1} |x_i| \\ k &= 1,2,\cdots,\tau \\ j &= 1,2,\cdots,\frac{N}{\tau} \end{aligned} \tag{4}$$

Step 2. Calculate the DE for each $y_{k,j}^{\tau}$ $(k=1,2,\cdots,\tau)$ sequence separately and then the final IRCMDE value for scale factor τ can be calculated by Eq. (5).

$$IRCMDE(u,m,c,d,\tau) = \frac{1}{\tau}\sum_{k=1}^{\tau} DE(y_k^{\tau},m,c,d) \tag{5}$$

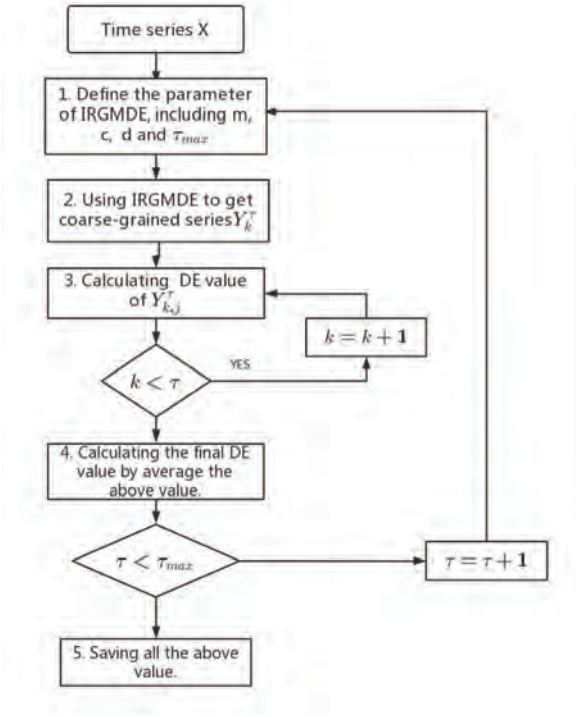

Fig. 1. the flowchart of the IRCMDE method

PARAMETER SELECTION AND ANALYSIS

When using the IRCMDE method to analyse data, there are five main parameters which need to be set in advance: signal length N, embedding dimension m, the number of classes c, time delay d and scale factor τ. According to the relevant reference, the time delay is usually selected as 1, which has no influence on the computational efficiency and reliability of the DE value. The scale factor τ is selected as 18, which will fully extract fault information at different scales. Because white Gaussian noise (WGN) and 1/f noise are two commonly occurring noises in nature, we decide to analyse the impact of the other four parameters on the DE results by using these two signals. The coefficient of variation (CV) value and Euclidean distance (ED) value are calculated for evaluating the effectiveness of the DE results. The CV equation is defined as standard deviation divided by the mean and ED value, as shown in Eq. (6).

$$ED = \sqrt{\sum_{i=1}^{\tau} (DE_1(i) - DE_2(i))^2} \tag{6}$$

where DE_1 and DE_2 denote WGN and 1/f noise IRCMDE values, respectively.

PARAMETER OF SIGNAL LENGTH

In order to analyse the influence of signal length N on the DE value, we select 20 times WGN and 1/f noise with lengths of 512, 1024, 2048 and 4096, respectively, for calculating the IRCMDE value. The results are shown in Fig. 2, Table 1, Table 2 and Table 3. Fig. 2 shows that the entropy values of both WGN and 1/f noise are very similar, which indicates that the signal length has little influence on the multiscale entropy value. Moreover, it can be seen from Tables 1-3 that, with increasing signal length, the CV value becomes smaller, the ED value becomes larger and time become longer. Overall, it is more reasonable when the signal length is 2048, so N is chosen to be equal to 2048 in this study.

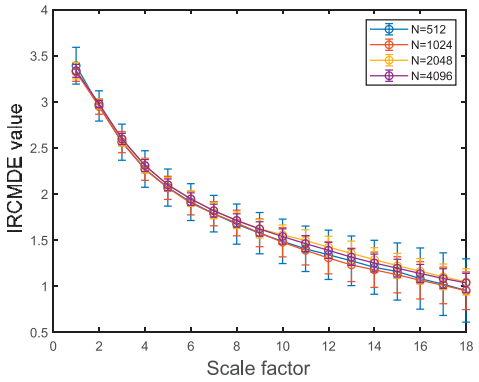

(a) Entropy value of WGN

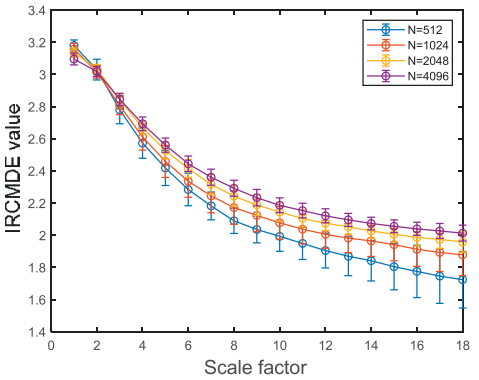

(b) Entropy value of 1/f noise

Fig. 2. IRCMDE value of different signal lengths

Table 1. CV value of different data lengths

Data length	512	1024	2048	4096
WGN	0.1732	0.1098	0.0703	0.0536
1/f noise	0.0537	0.0429	0.0224	0.0190

Table 2.Consuming time with different data lengths

Data length	512	1024	2048	4096
WGN	0.0950s	0.0879s	0.1288s	0.2130s
1/f noise	0.0851s	0.1138s	0.1203s	0.2134s

Table 3. ED value with different data lengths

Data length	512	1024	2048	4096
ED	2.0693	2.6295	2.6430	2.8253

PARAMETER OF EMBEDDING DIMENSION

The embedding dimension *m* has a great influence on the entropy value. If *m* is too small, the dynamic information from the signal may not be detected. If *m* is too large, the small variations in the signal may not be displayed and it is also more time-consuming. Therefore, we decided to select *m* values equal to 2, 3, 4 and 5, respectively, for calculating the IRCMDE value. The calculation results are shown in Fig. 3, Table 4, Table 5 and Table 6. Fig. 3 shows that the entropy value will become larger with an increase of embedding dimension *m*. This is because there will be more dispersion patterns when *m* is larger, and so a larger DE value will be produced. Moreover, it can be seen from Tables 4-6 that, when *m* is equal to 3, the CV value is relatively lower, the consuming time is relatively shorter and the ED value is relatively longer. So, an embedding dimension *m* of 3 was chosen in this study.

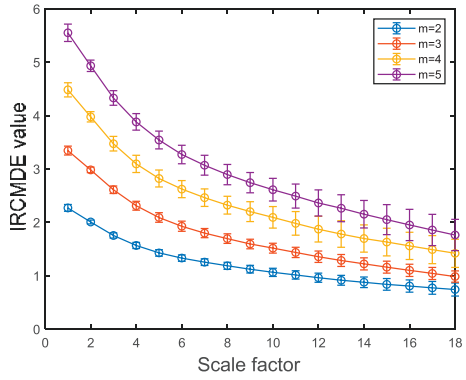

(a)b Entropy value of WGN

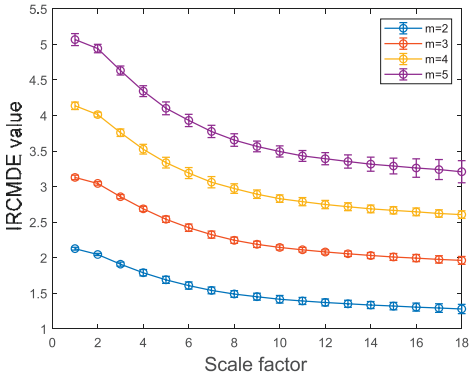

(b) Entropy value of 1/f noise

Fig. 3. IRCMDE values of different embedding dimensions

Table 4. CV values of different embedding dimensions

Embedding dimension	2	3	4	5
WGN	0.0738	0.0805	0.0552	0.0883
1/f noise	0.0311	0.0258	0.0215	0.0260

Table 5. Time consumed with different embedding dimensions

Embedding dimension	2	3	4	5
WGN	0.0721s	0.1223s	0.4427s	2.2708s
1/f noise	0.0695s	0.1151s	0.4292s	2.2589s

Table 6. ED values with different embedding dimensions

Embedding dimension	2	3	4	5
ED	1.7316	2.5567	3.2294	3.6448

THE NUMBER OF CLASS C

The parameter c is one of the important parameters determining the number of dispersion patterns. When c is too small, there are not enough patterns to reflect signal information, resulting in two signals with different amplitudes being divided into the same class. However, when c is too large, the calculation time will become very long and the signal may be divided into different classes when encountering noise pollution. Therefore, we decided to select c equal to 4, 5, 6 and 7, respectively, for calculating IRCMDE values. The calculation results are shown in Fig. 4, Table 7, Table 8 and Table 9. Fig. 4 shows that the entropy value will increase with the increase in class number because there will be more possible dispersion patterns under a larger class number c. In other words, when c is larger, there will be more information which can be extracted, yielding a larger DE value. However, when c is larger, the calculation time will become longer and the ED value will become shorter. Therefore, after comprehensive analysis, a c value of 6 was chosen, which is more reasonable.

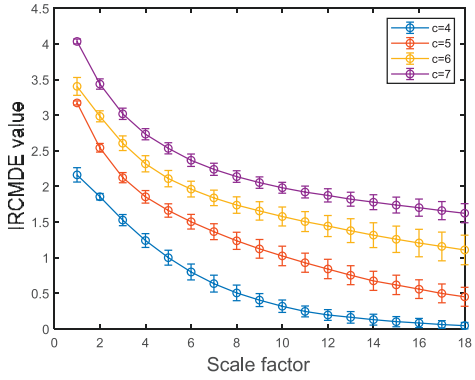

(a) Entropy values of WGN

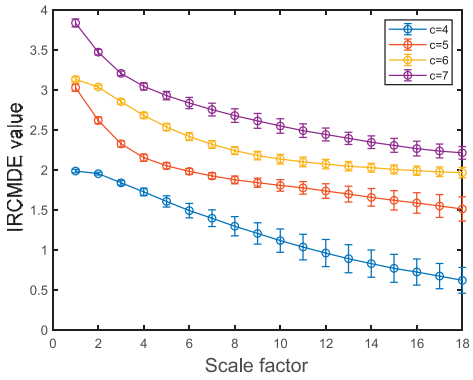

(b) Entropy values of 1/f noise

Fig.4. IRCMDE values of different class numbers

Table 7. CV values of different class numbers

Class number	4	5	6	7
WGN	0.2603	0.1507	0.0566	0.0495
1/f noise	0.1018	0.0508	0.0284	0.0224

Table 8. Consuming time with different class numbers

Class number	4	5	6	7
WGN	0.0819s	0.1257s	0.1627s	0.2556s
1/f noise	0.1033s	0.1051s	0.1472s	0.1538s

Table 9. ED values with different class numbers

Class number	4	5	6	7
ED	2.6069	3.5288	2.4144	1.8705

COMPARISON OF IRCMDE, RCMDE, MDE AND MPE

When a fault occurs, the fault signal usually contains modulation components. Our research selected five AM-FM signals containing different frequencies and amplitudes as simulation signals, as shown in Eq. (7) [31].

$$x = (1 + a * \cos(6\pi t)) * \cos(b * 20\pi t + 2 * \cos(10\pi t)) + \\ + c * (0.8\sin(\pi t) * \sin(30\pi t)) \tag{7}$$

The sample frequency is 2048 Hz, and a, b, and c are coefficients forming five different modulation signals, which are expressed as a=[0.5,1,1.5,2,2.5], b=[1,2,3,4,5], and c=[1,2,3,4,5].

The calculation results are shown in Fig 5. It can be seen that the DE values of the five signals have obvious intersections when using the MDE method. The entropy value of IRCMDE and RCMDE are separated on most scales. This indicates that multi-scale analysis is very important when evaluating the information from practical fault signals, which is beneficial for achieving fault diagnosis in mechanical equipment.

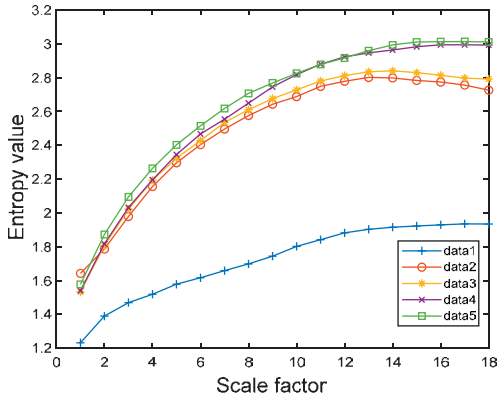

(a) Entropy values of IRCMDE

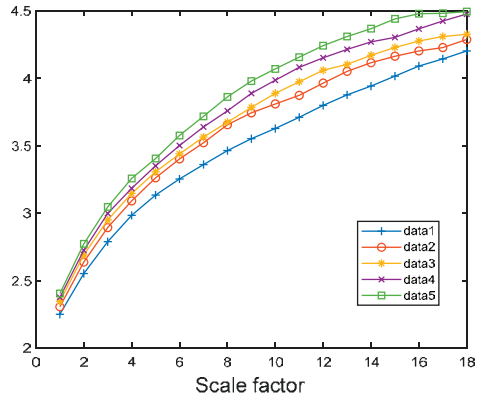

(b) Entropy values of RCMDE

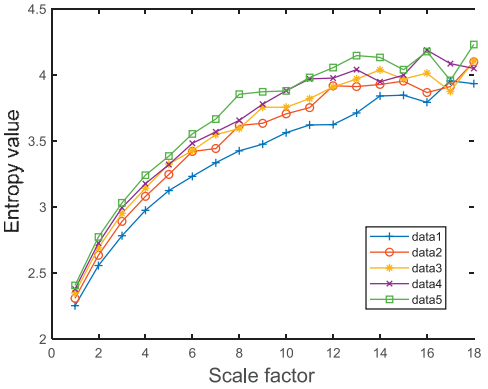

(c) Entropy values of MDE

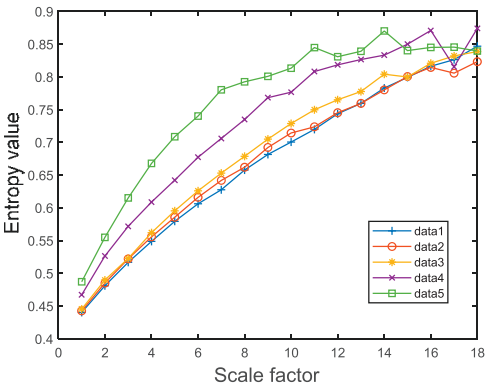

(d) Entropy values of MPE

Fig. 5. Entropy values of five modulation signals

When an engine's fuel injection system appears to have faults, the measured signal is often affected by background noise. Therefore, five different levels of signal to noise ratio (SNR) were used to form a synthetic signal, with the aim of further demonstrating the noise reduction ability of the proposed algorithm. The SNRs used were: 10, 15, 20 and 25. Fig. 6 shows the calculation results of entropy value from the four methods, using synthetic signals. It can been seen that, when the SNR is different, there are fluctuations and severe crossovers between different scales in the IRCMDE, MDE and MPE entropy curves, but the IRCMDE entropy is much smoother. Therefore, the IRCMDE method has a better noise reduction effect and is more suitable for the feature extraction of actual signals.

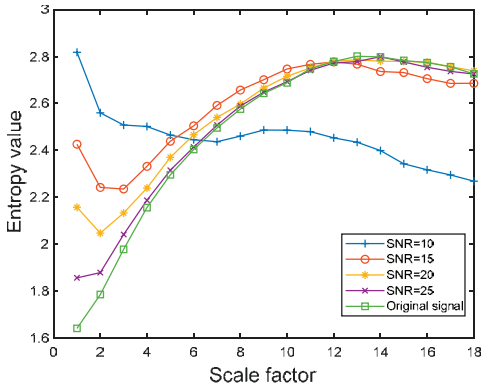

(a) Entropy values of IRCMDE

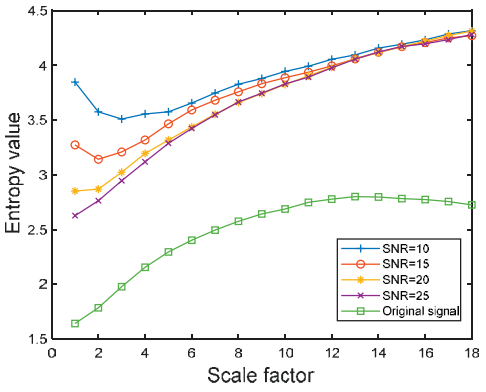

(b) Entropy values of RCMDE

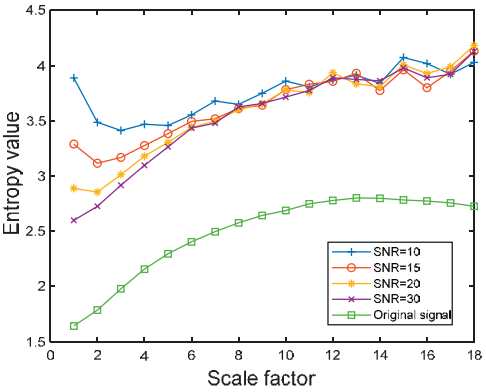

(b) Entropy values of MDE

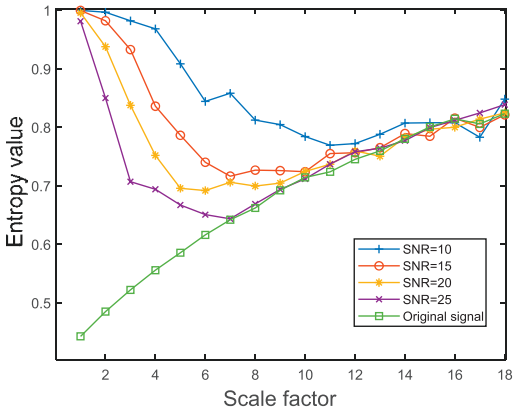

(d) Entropy values of MPE

Fig. 6. Entropy values of five modulation signals

THE PROPOSED FAULT DIAGNOSIS METHOD

FAST CORRELATION-BASED FILTER FOR FEATURE SELECTION

Fault diagnosis is required after feature extraction. However, if all of these features are used, the classification accuracy rate may not be high and the calculation time is also very long. Therefore, the feature selection method is needed for further improving the effectiveness of fault diagnosis. Fast correlation-based filter (FCBF) is one of the most widely used non-liner correlation measures, which is used for feature selection [32].

Definition 1. Information entropy solves the measurement of complexity of random information variables. If X is a discrete signal, then the entropy of X is expressed as:

$$H(X) = -\sum_{i=1}^{n} p(x_i) \log p(x_i) \tag{8}$$

Definition 2. The conditional entropy is expressed as the conditional probability distribution of the occurrence of random variable X when random variable Y occurs alone.

$$H(X \mid Y) = -\sum p(y) \sum p(x \mid y) \log p(x \mid y) \tag{9}$$

Definition 3. Mutual information of discrete signal X and Y can be defined as:

$$I(X,Y) = H(X) - H(X \mid Y) \tag{10}$$

From Eq. (10), it can be seen that the upper limit of *I(X,Y)* is the minimum value between *H(X)* and *H(Y)*, and its lower limit is 0. Due to the significant variation in entropy, uncertain entropy values can lead to unreasonable values of *I(X,Y)*. Therefore, it is necessary to process the maximum information coefficient of *I(X,Y)* because the maximum information coefficient can compensate for the deviation of mutual information in the multi value feature, and limit its value range to [0, 1]. Therefore, the maximum information coefficient of random variables X and Y can be determined by the minimum value of *H (X)* and *H (Y)*, as shown below.

$$I_{\max}(X,Y) = \frac{I(X,Y)}{\min(H(X), H(Y))} \tag{11}$$

Definition 4. Symmetrical uncertainty (SU) is defined as:

$$SU_{\max}(X,Y) = \frac{2I_{\max}(X,Y)}{H(X) + H(Y)} \tag{12}$$

In order to reduce the redundancy between signal features, the calculation steps of the FCBF method are as follows:

Step 1: Calculation the $SU_{max}(x_i,c)$ value for each feature x_i, where i the i-th feature and c is the class vector.

Step 2: Delete the irrelevant feature x_i, whose $SU_{max}(x_i,c) < \delta$, where δ is a predefined threshold.

Step 3. List the remaining features in descending order, according to their SU_{max} value and label the result as S_{list}.

Step 4. Define the first element x_m in S_{list} as the predominant feature, append x_m to s_{select} and remove it from S_{list}. For the remaining features, calculate the $SU_{max}(x_m,x_n)$. Remove redundant features based on conditions similar to Markov blankets. So, if $SU_{max}(x_m,x_n) > SU_{max}(x_n,c)$ and $SU_{max}(x_m,c) > SU_{max}(x_n,c)$, remove x_n from s_{list}.

Step 5. Regard the remaining feature next to x_m in the S_{list} as the new predominant feature and repeat step 4 until $S_{list} = \phi$. Finally, the relevant but non-redundant feature set s_{select} is obtained.

SUPPORT VECTOR MACHINE FOR FAULT CONDITION RECOGNITION

For an ME marine diesel engine, the fault sample is relatively insufficient. SVM as one of the supervised classifiers which is especially suitable for small sample cases; it is based on the principle of minimising the structural risk in statistical learning theory. SVM was originally developed for binary classification problems. However, the fault diagnosis of a marine diesel engine is usually a multi-classification problem. To address this issue, one-verse-one and one-verse-all are proposed. According to the literature [33], researchers decided to select the style of one-verse-one mode method and optimise parameter g and the penalty parameter c through particle swarm optimisation (PSO).

THE PROPOSED FAULT DIAGNOSIS METHOD

In order to realise the fault diagnosis of an ME diesel engine, a novel fault diagnosis method based on IRCMDE, FBCF and SVM is proposed in this paper. The flowchart of the proposed method is displayed in Fig. 7 and the calculating steps of the method are described as follows.

Step 1: Signal acquisition. Installing the relevant transducer to collect the signal under different working conditions. In this research, we installed a pressure and vibration transducer on the high pressure oil pipe of an ME diesel engine.

Step 2: Feature extraction. The IRCMDE method was used to extract the fault feature from the raw signal.

Step 3. Feature selection. The FCBF method was used to select the more sensitive features.

Step 4. Condition classification. The SVM method was used to classify the fault conditions.

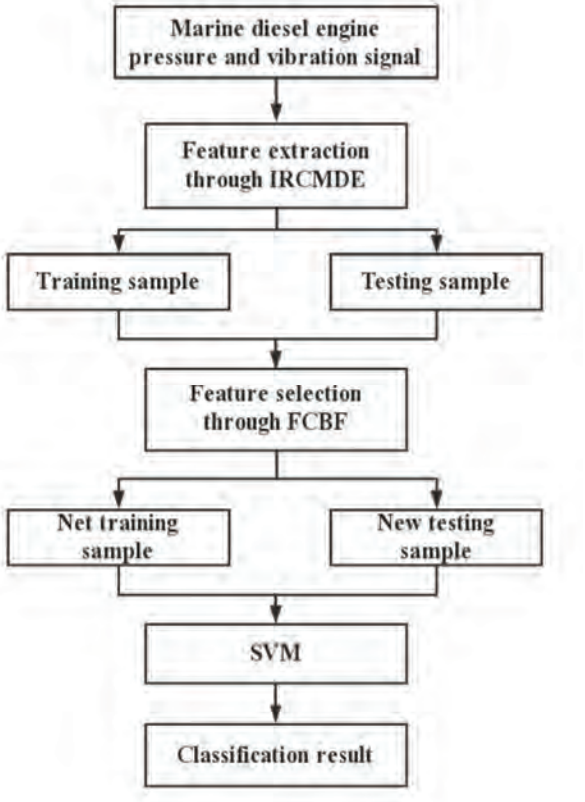

Fig. 7. Flowchart of the proposed method

EXPERIMENTAL VERIFICATION

EXPERIMENTAL SETUP DESCRIPTION AND DATA COLLECTION

To verify the effectiveness and applicability of the proposed method, experiments on an ME diesel engine were conducted. The ME diesel engine was located in Shanghai Maritime University Automation Engine Room Laboratory, as shown in Fig. 8. I was a MAN B&W 6S35ME-B9 type engine and the main parameters are listed in Table 10.

Table 10. Main parameters of ME diesel engine

Number	Parameter	Value
1	Number of strokes	2
2	Firing sequence	1-5-3-4-2-6
3	Rated Power	3570 kW
4	Rated speed	140 r/min
5	Compression ratio	21
6	Cylinder bore/Stoke	350 mm/1550 mm
7	Connecting rod length	1550 mm
8	Intake mode	Supercharging cooling

(a)

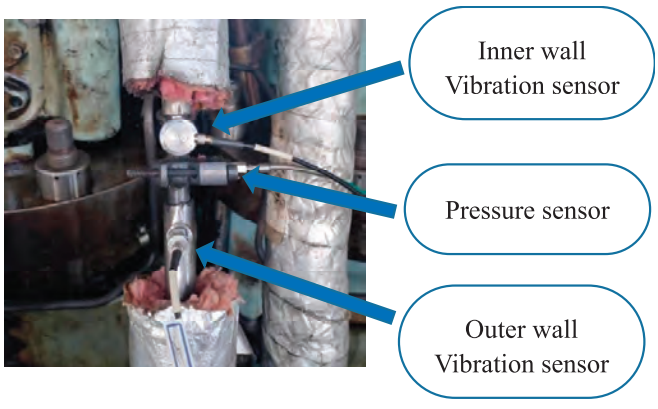

(b)

Fig. 8. Experimenalt rig

The fuel injector is the part of the fuel injection system most prone to malfunction, therefore three common injector failures, including reduced pressure at the opening valve, clogged spray holes and worn needle valves, were experimentally studied. In general, the vibration signal of the high-pressure fuel line was measured to obtain fault

information [34]. However, for ME diesel engines, the high-pressure fuel pipe is a double-walled pipe with a channel between the walls for oil return, in case of leakage. In addition, because the pressure in high-pressure oil pipes can sometimes reach 100 MPa, a double-walled structure is also beneficial for increasing safety. This double-wall construction leads to the possibility of inaccurate fault diagnosis by measuring the vibration signal on the outer wall of the high-pressure fuel pipe. Therefore, in this experiment, the pressure signal was measured by drilling holes in the inner wall of the high-pressure oil pipe. The pressure sensor model used for the experiment was a Kistler 4067E3000DS with a maximum measurement range of 300 MPa. For the comparison study, the vibration signals of the inner and outer walls of the high-pressure fuel line were measured simultaneously. During the experiment, in order to improve safety and prevent the high-pressure oil pipe from bursting at the perforation, woven bags were used for wrapping, as shown in the red box in Fig. 8(a). Fig. 8(b) is the detailed sensor installation location diagram, including one pressure sensor and two vibration sensors. The signals are collected by a PC via a COINV system. The speed of the main bearing was set at 90 r/min and 30% rated power, and the sampling rate was 2048 Hz. The sampling time for each condition lasted 50 s, i.e. there were 50*2048 points under each working condition. In order to validate the proposed method, all of the 102,400 points were selected as the sample sets. According to the analysis in Section 3, there are 2048 points per sample, so there are 50 samples per working state. Moreover, we randomly selected 30 samples as the training set and the remaining 20 samples as the test set. Thereby, a total of 120 training samples and 80 testing samples could be acquired. A detailed description of the fuel injector working condition is shown in Table 11.

Table 11. Detailed description of the fuel injector working condition

Working condition	Training samples	Testing samples	Label
Normal	30	30	1
Low valve opening pressure	30	30	2
Orifice blockage	30	30	3
Needle valve wear	30	30	4

The time-domain waveform of each working condition is shown in Fig. 9-12 and each state contains 3 graphics, including pressure waveform, inner wall vibration waveform and outer wall vibration waveform, from top to bottom. It can be seen that different working conditions have similar waveforms, so it is necessary to apply the intelligent fault diagnosis method to accurately identify different working conditions. Moreover, the instantaneous pressure of fuel injection can reach up to 70 MPa and the vibration is also the most severe at this time. However, based on our experience, the vibration signal of the outer wall is more susceptible to external interference and contains more high-frequency noise. In order to verify which type of signal enables better injector fault diagnosis, a comparative analysis was carried out later, using pressure signals and vibration signals, respectively.

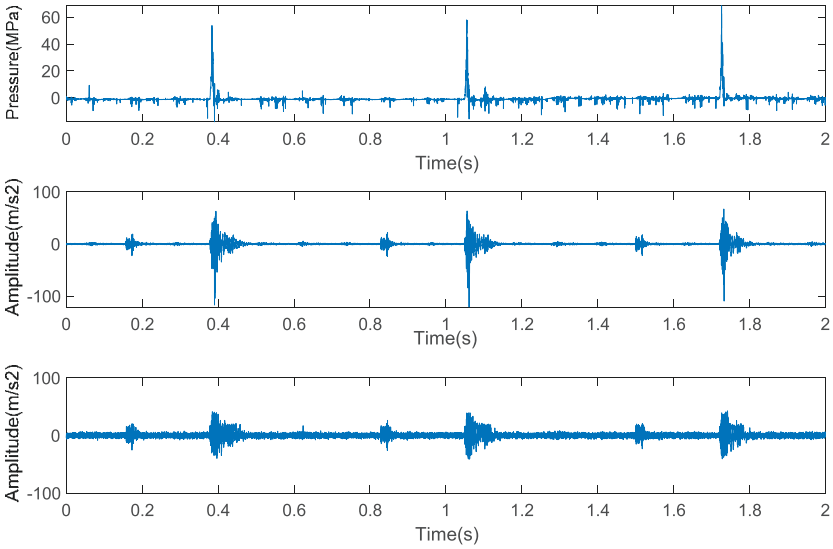

Fig. 9. Time domain waveform of signal under normal condition

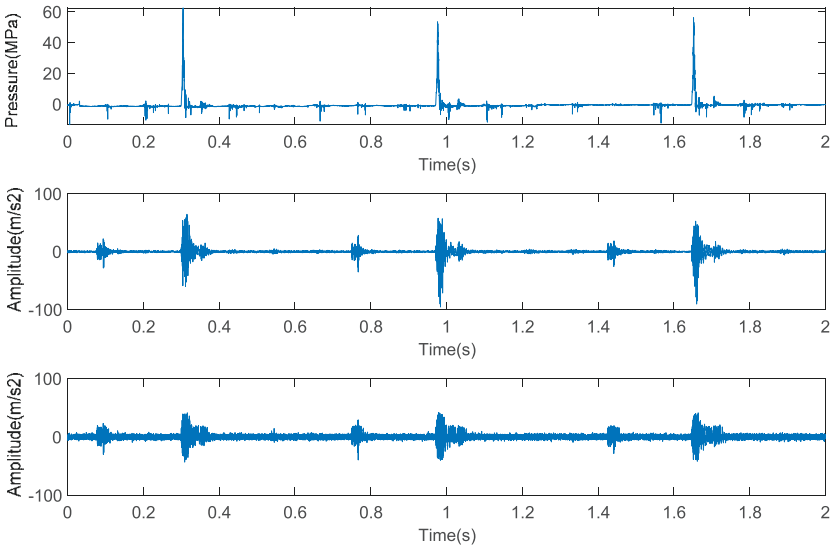

Fig. 10. Time domain waveform of signal under low valve opening pressure

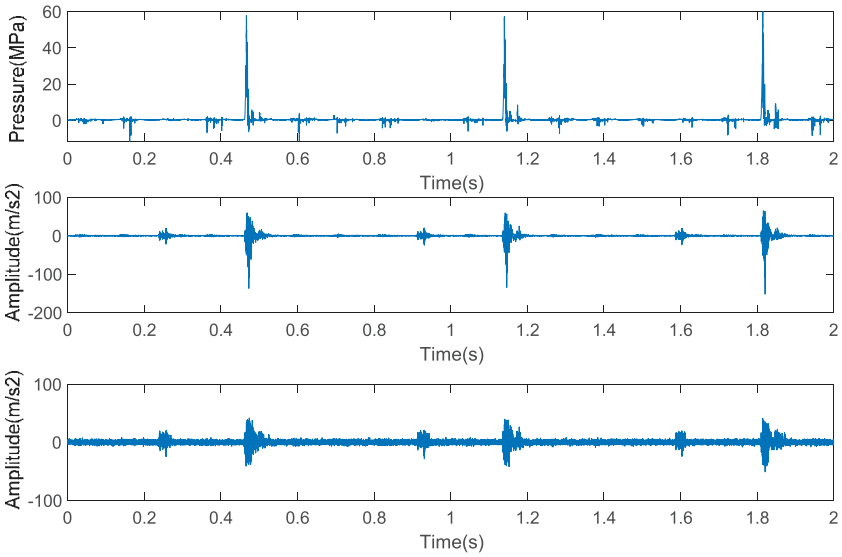

Fig. 11. Time domain waveform of signal under orifice blockage

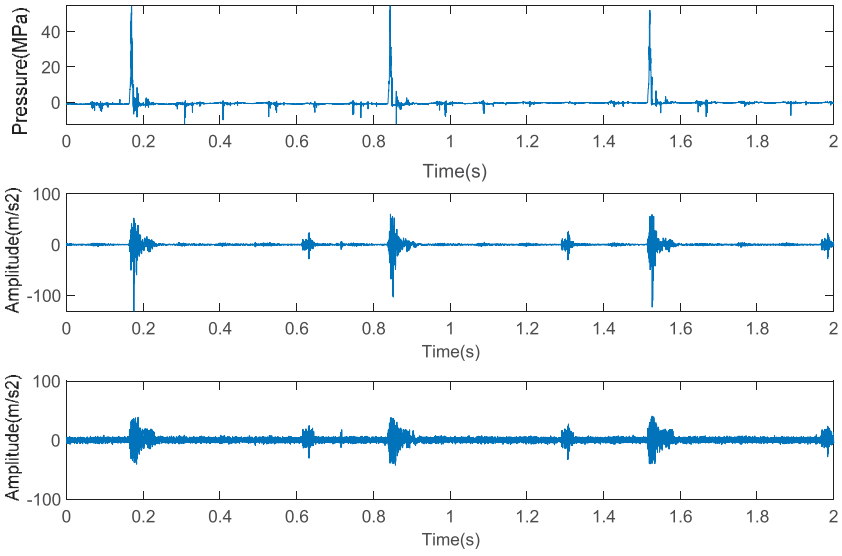

Fig. 12. Time domain waveform of signal under needle valve wear

DIAGNOSIS RESULTS AND ANALYSIS

According to the flowchart of the proposed method in Fig 7, IRCMDE is first used to extract the fault features from the fuel injection pressure signal and the calculation results of each extracted multi-scale features is shown in Fig. 13. It can be seen that the entropy values are different under most working conditions. However, in the cases of condition 1 and condition 3, the entropy curve shows a cross phenomenon because, when the injector nozzle is blocked, it will cause an increase in valve opening pressure. However, the blockage of the nozzle will generally be accompanied by a decrease in valve opening spring stiffness, both of which cause the valve opening pressure to be consistently normal. Therefore, the entropy value of the pressure wave is also approximately the same. Meanwhile, condition 4 has the maximum entropy value at all scales, indicating that needle valve wear faults contain more information. In order to verify the effect of needle valve wear on injector performance, the injector was tested on the injector opening pressure test rig and found to have very large fluctuations in opening pressure. This unstable operating condition resulted in a larger entropy value as well.

Because each sample has eighteen features, some of them may affect classification accuracy, due to interference. It is necessary to reduce the dimension of the feature set. Therefore, FCBF is used to select the main features according to their superiority and correlations. As a comparison, three entropy methods including RCMDE, MDE and MPE are also calculated, and FCBF is used to calculate the sensitivity on all the scales of the above methods. Table 12 shows the main features of the different methods. Then, the selected training sample of entropy values were used to train the SVM model and the selected testing sample entropy values were used to test the model. Before training SVM, the parameters of penalty factor c and kernel function parameter g need to be set. Here, we decides to use PSO to obtain the optimal parameters and the PSO theory can be found in the literature [35]. After 60 iterations, the optimal parameters c=10 and g=1 were obtained. The detailed fault diagnosis results can be seen from the confusion matrix, as is shown in Fig. 14. The proposed method of IRCMDE has the highest fault diagnosis rate, with an accuracy rate of 91.25%. The accuracy rates of the other three methods are 88.75%, 81.25% and 78.75%, respectively. As can been seen from the four methods above, fault condition 2 had the lowest classification accuracy. This is because, after long-term operation of marine diesel engines and frequent use of heavy oil, the internal spring stiffness of the fuel injector will naturally decrease, resulting in a lower valve opening pressure. So the failure of reducing valve opening pressure can easily cause confusion with other faults.

Table 12. Main features of the different methods.

Method	Feature scale			
IRCMDE	18	6	10	2
RCMDE	11	18	4	7
MDE	8	10	3	6
MPE	5	16	8	12

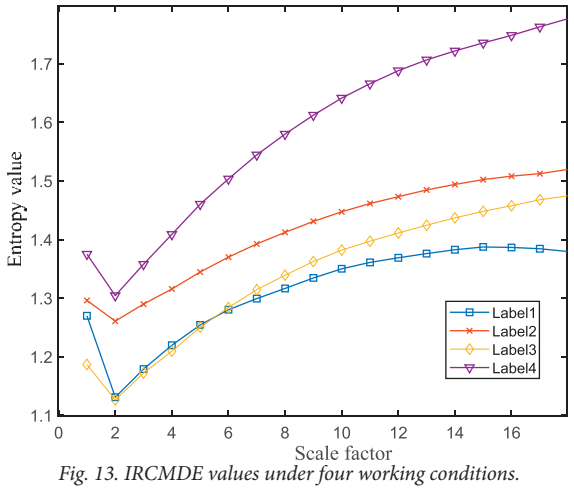

Fig. 13. IRCMDE values under four working conditions.

To further validate the effectiveness of the proposed algorithm, the fault diagnosis rate of each method was calculated twenty times, and the results are shown in Fig. 15. Five comparative indexes of the four methods in 20 trials are listed in Table 13, which includes the maximum, minimum, mean, SD and calculation time of accuracy for 20 trials. From Fig. 15 and Table 13, it can be concluded that the proposed method has the best accuracy and the SD value is relatively smaller. That indicates that the proposed method not only has better classification accuracy, but is also more stable. There are several reasons for the illustrated comparative results. Firstly, PE is greatly affected by the signal amplitude while DE improves stability through nonlinear mapping. Secondly, IRCMDE and RCMDE fully consider the relationship between adjacent elements at each scale and generate more template vectors for short-term time series. Besides this, IRCMDE also considers the relative energy between the signals.

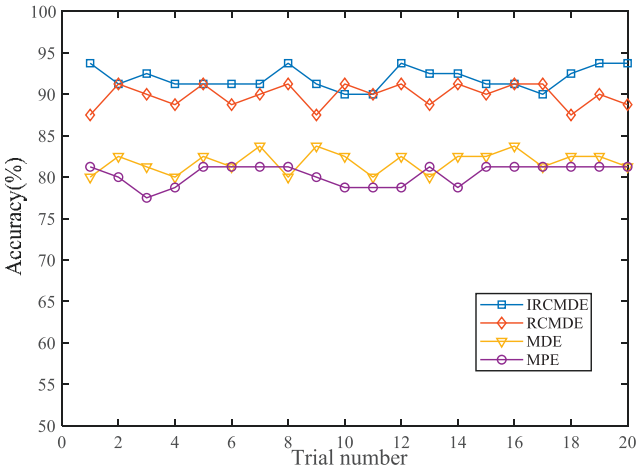

Fig. 15. Accuracy of four methods

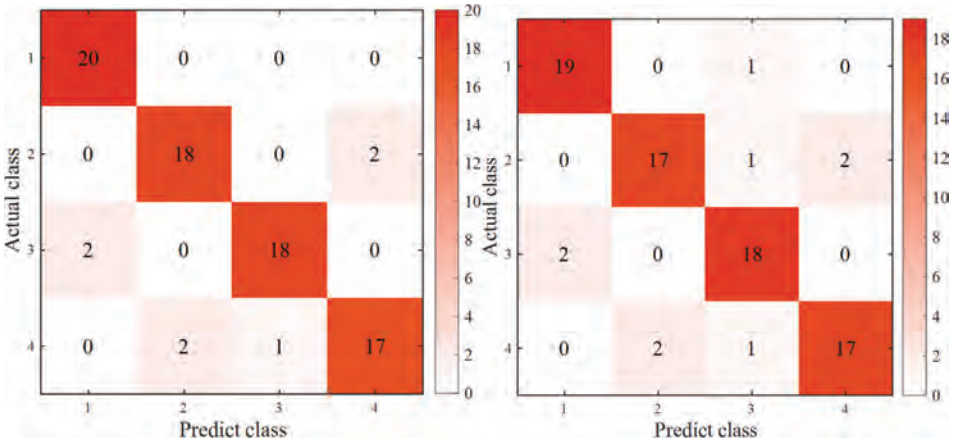

(a) IRCMDE *(b) RCMDE*

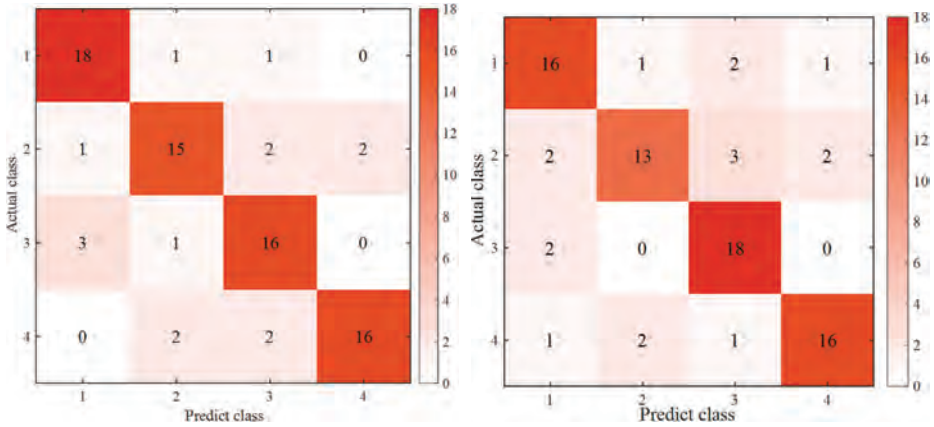

(c)MDE *(d) MPE*

Fig. 14. Multi-class confusion matrix of different methods.

Table 13. Comparative indexes of different methods

Method	Comparative indexes			
	Maximum	Minimum	Mean	SD
IRCMDE	93.75	90.0	92.12	1.0512
RCMDE	91.25	87.5	89.50	1.3079
MDE	83.75	80.0	81.75	1.7396
MPE	81.25	77.5	78.94	1.6351

COMPARATIVE ANALYSIS OF USING PRESSURE AND VIBRATION SIGNALS

It can be seen, from Fig. 9 to 12, that, when the pressure in the high-pressure oil pipe increases, the vibration signal will also be significantly enhanced. However, the vibration signal is more susceptible to the influence of other cylinders. For example, there are two significant increases in the vibration signal waveform within a working cycle. Because our experiment was conducted on cylinder 1 at a speed of 90 r/min, it can be concluded that the most obvious vibration is the process of fuel injection and ignition in cylinder 1. According to the ignition sequence 1-5-3-6-2-4, the second most obvious vibration signal is the process of fuel injection and ignition in cylinder 2. As a comparison, inner wall vibration signals and outer wall vibration signals of the double-walled high pressure fuel pipe were used to diagnose fuel injector faults. As can be seen from Fig. 16, there is a phenomenon of entropy crossover, and the entropy crossover of the outer wall vibration signal is particularly severe. This means that the feature differentiation is not clear enough, which is not conducive to fault classification. A confusion matrix showing the effects of fault diagnosis is shown in Fig. 17, where the outer wall's fault diagnosis rate is 47.5% and the inner wall's fault diagnosis accuracy rate is 61.25%. This demonstrates that fault diagnosis in injectors is not well achieved using high pressure fuel pipe vibration signals. To explain this phenomenon, the high-pressure fuel pipe was sawn off and, as a result, the wall thickness of the inner pipe was found to be as high as 5 mm by measurement; the gap between the inner pipe and the outer pipe was 1 mm. This structure of the high-pressure tube improved the operational safety, to a certain extent but, on the other hand, it also weakened the internal pressure transmission of the high-pressure tube. Therefore, the accuracy of fault diagnosis based on vibration signals is relatively low.

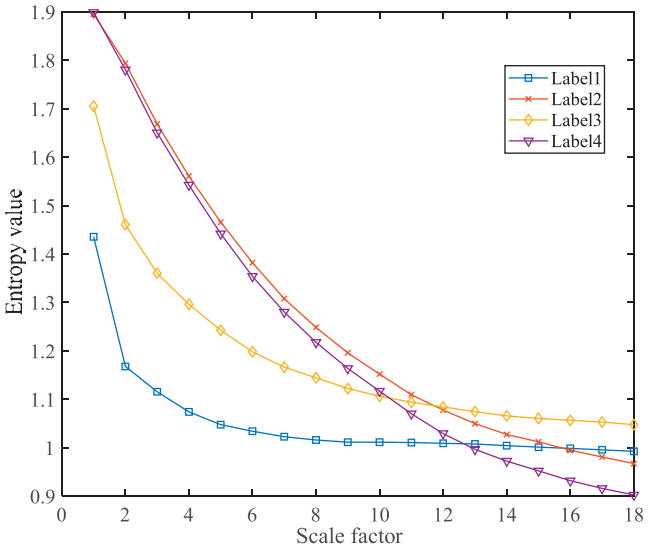

(a) Entropy value of inner tube vibration signal

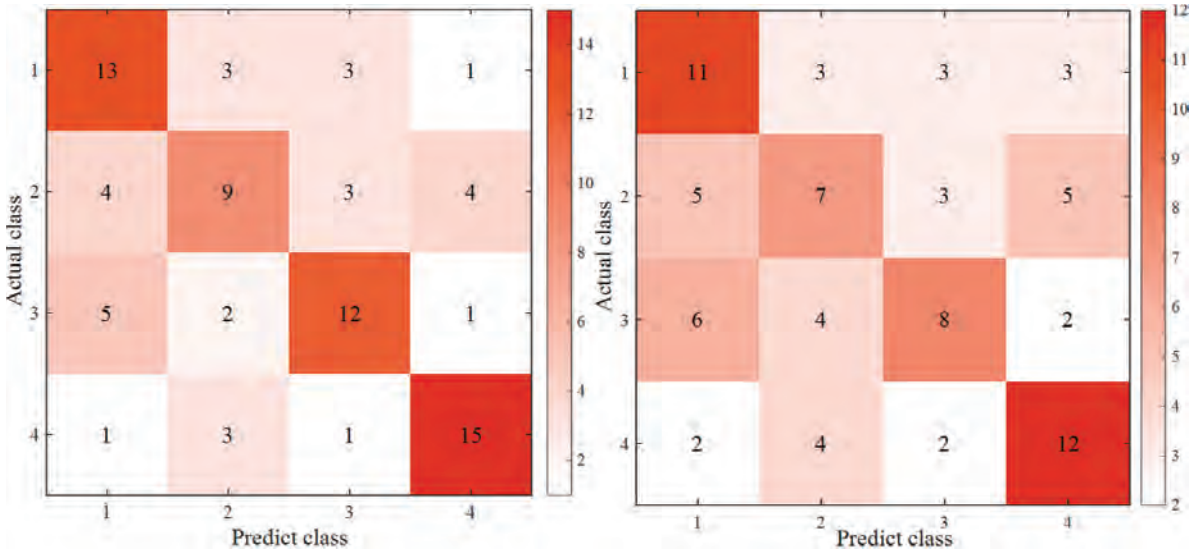

(a) Inter- tube vibration signal *(b) Outer tube vibration signal*

Fig. 17. Multiclass confusion matrix of different vibration signals

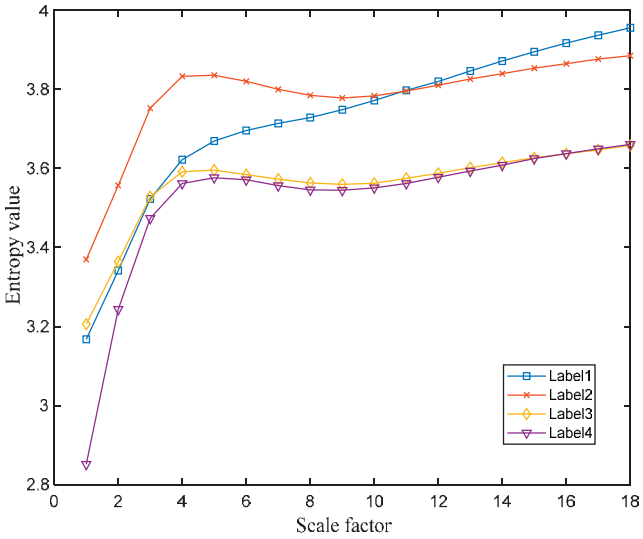

(b) Entropy value of outer tube vibration signal

Fig. 16. IRCMDE values of different vibration signals

CONCLUSION

Considering the non-stationary and nonlinear characteristics of the fuel injection pressure signal and vibration signal of a high-pressure fuel pipe, a novel intelligent fault diagnosis method, based on IRCMDE and FCBF, is proposed. The IRCMDE can extract more fault features from the original different working condition signals, which is beneficial for improving the accuracy of fault diagnosis. Then, FCBF should be used to select the sensitive features and SVM employed to classify the working condition. The main contribution of this paper can be concluded as follows:

It is the firstly time the fuel injection pressure signal has been measured on a large marine two-stroke MAN B&W 6S35ME-B9 diesel engine. The literature showed that most research has been carried out based on four-stroke diesel engines. Besides this, some research was based on model simulation to study fuel injector faults. (2) In this manuscript, IRCMDE is proposed, which overcomes the neutralisation phenomenon during the coarse-graining process. It can extract feature information from the complex signal more effectively and its parameter selection criterion has also been discussed in detail. The superiority of IRCMDE is validated using both simulation and experimental signals, compared with RCMDE, MDE, and MPE. (3) It is also the first time that both the fuel injection pressure signal and vibration signal of a high-pressure fuel pipe has been measured simultaneously on a marine two-stroke large diesel engine, in states such as reduced injector opening valve pressure, blocked spray holes, and worn needle valves. The experimental results showed that 92.15% fault diagnosis accuracy could be achieved for the pressure signal using IRCMDE; however, vibration signals of the inner and outer wall of the high pressure fuel pipe could only reach 61.25% and 47.5%, respectively.

ACKNOWLEDGEMENTS

This work was supported by the Science & Technology Commission of Shanghai Municipality and Shanghai Engineering Research Center of Ship Intelligent Maintenance and Energy Efficiency, under Grant 20DZ2252300.

DECLARATION OF COMPETING INTERESTS

The authors declare that they have no known competing financial interests or personal relationships that could have appeared to influence the work reported in this paper.

REFERENCES

1. C.G. Rodriguez, M.I. Lamas, J.D. Rodriguez and A. Abbas, "Analysis of the Pre-Injection System of a Marine Diesel Engine Through Multiple-Criteria Decision-Making and Artificial Neural Networks," Pol. Marit. Res., vol. 28, no. 4, pp. 88-96, 2022, doi: 10.2478/pomr-2021-0051.

2. F. Gao, "An integrated risk analysis method for tanker cargo handling operation using the cloud model and DEMATEL method," Ocean Eng., vol. 266, pp. 113021, 2022, doi: 10.1016/j.oceaneng.2022.113021.

3. R. Varbanets, et al., "Concept of Vibroacoustic Diagnostics of the Fuel Injection and Electronic Cylinder Lubrication Systems of Marine Diesel Engines," Pol. Marit. Res., vol. 29, no. 4, pp. 88-96, 2022, doi: 10.2478/pomr-2022-0046.

4. J. Kowalski, "An Experimental Study of Emission and Combustion Characteristics of Marine Diesel Engine with Fuel Injector Malfunctions," Pol. Marit. Res., vol. 23, no. 1, pp. 77-84, 2016, doi: 10.1515/pomr-2016-0011.

5. M.G. Thurston, M.R. Sullivan and S.P. McConky, "Exhaust-gas temperature model and prognostic feature for diesel engines," Appl. Therm. Eng., vol. 229, pp. 120578, 2023, doi: 10.1016/j.applthermaleng.2023.120578.

6. Y. Li, W. Zhou and Y. Zi, "A graphic pattern feature-mapping-based data-driven condition monitoring method for diesel engine malfunction identification and classification," Proceedings of the Institution of Mechanical Engineers, Part C: Journal of Mechanical Engineering Science, vol. 233, no. 1, pp. 202-212, 2019, doi: 10.1177/0954406218755186.

7. M. Zhang, Y. Zi, L. Niu, S. Xi and Y. Li, "Intelligent Diagnosis of V-Type Marine Diesel Engines Based on Multifeatures Extracted From Instantaneous Crankshaft Speed," IEEE T. Instrum. Meas., vol. 68, no. 3, pp. 722-740, 2019, doi: 10.1109/TIM.2018.2857018.

8. Y. Yang, A. Ming, Y. Zhang and Y. Zhu, "Discriminative non-negative matrix factorisation (DNMF) and its application to the fault diagnosis of diesel engine," Mech. Syst. Signal Pr., vol. 95, pp. 158-171, 2017, doi: 10.1016/j.ymssp.2017.03.026.

9. E. Ftoutou and M. Chouchane, "Diesel engine injection faults' detection and classification utilizing unsupervised fuzzy clustering techniques," Proceedings of the Institution of Mechanical Engineers, Part C: Journal of Mechanical Engineering Science, vol. 233, no. 16, pp. 5622-5636, 2019, doi: 10.1177/0954406219849089.

10. S.M. Ramteke, H. Chelladurai and M. Amarnath, "Diagnosis of Liner Scuffing Fault of a Diesel Engine via Vibration and Acoustic Emission Analysis," Journal of Vibration Engineering & Technologies, vol. 8, no. 6, pp. 815-833, 2020, doi: 10.1007/s42417-019-00180-7.

11. A. Zabihi-Hesari, S. Ansari-Rad, F.A. Shirazi and M. Ayati, "Fault detection and diagnosis of a 12-cylinder trainset diesel engine based on vibration signature analysis and neural network," Proceedings of the Institution of Mechanical Engineers, Part C: Journal of Mechanical Engineering Science, vol. 233, no. 6, pp. 1910-1923, 2019, doi: 10.1177/0954406218778313.

12. L. Li, S. Tiexiong, F. Ma and Y. Pu, "Research on a small sample fault diagnosis method for a high-pressure common rail system," Advances in Mechanical Engineering, vol. 13, no. 9, pp. 2072279549, 2021, doi: 10.1177/16878140211046103.

13. A. Zabihi-Hesari, S. Ansari-Rad, F.A. Shirazi and M. Ayati, "Fault detection and diagnosis of a 12-cylinder trainset diesel engine based on vibration signature analysis and neural network," Proceedings of the Institution of Mechanical Engineers, Part C: Journal of Mechanical Engineering Science, vol. 233, no. 6, pp. 1910-1923, 2019, doi: 10.1177/0954406218778313.

14. A. Taghizadeh-Alisaraei and A. Mahdavian, "Fault detection of injectors in diesel engines using vibration time-frequency analysis," Appl. Acoust., vol. 143, pp. 48-58, 2019, doi: 10.1016/j.apacoust.2018.09.002.

15. Y. Chen, T. Zhang, Z. Luo and K. Sun, "A Novel Rolling Bearing Fault Diagnosis and Severity Analysis Method," Applied Sciences, vol. 9, no. 11, pp. 2356, 2019, doi: 10.3390/app9112356.

16. Y. Shang, G. Lu, Y. Kang, Z. Zhou, B. Duan and C. Zhang, "A multi-fault diagnosis method based on modified Sample Entropy for lithium-ion battery strings," J. Power Sources, vol. 446, pp. 227275, 2020, doi: 10.1016/j.jpowsour.2019.227275.

17. K. Zhu and H. Li, "A rolling element bearing fault diagnosis approach based on hierarchical fuzzy entropy and support vector machine," Proceedings of the Institution of Mechanical Engineers, Part C: Journal of Mechanical Engineering Science, vol. 230, no. 13, pp. 2314-2322, 2016, doi: 10.1177/0954406215593568.

18. Y. Ma, J. Cheng, P. Wang, J. Wang and Y. Yang, "Rotating machinery fault diagnosis based on multivariate multiscale fuzzy distribution entropy and Fisher score," Measurement, vol. 179, pp. 109495, 2021, doi: 10.1016/j.measurement.2021.109495.

19. C. Ma, Y. Li, X. Wang and Z. Cai, "Early fault diagnosis of rotating machinery based on composite zoom permutation entropy," Reliab. Eng. Syst. Safe., vol. 230, pp. 108967, 2023, doi: 10.1016/j.ress.2022.108967.

20. S. Wu, P. Wu, C. Wu, J. Ding and C. Wang, "Bearing Fault Diagnosis Based on Multiscale Permutation Entropy and Support Vector Machine," Entropy-Switz., vol. 14, no. 8, pp. 1343-1356, 2012, doi: 10.3390/e14081343.

21. Y. Li, G. Li, Y. Wei, B. Liu and X. Liang, "Health condition identification of planetary gearboxes based on variational mode decomposition and generalised composite multi-scale symbolic dynamic entropy," Isa T., vol. 81, pp. 329-341, 2018, doi: 10.1016/j.isatra.2018.06.001.

22. H. Azami and J. Escudero, "Amplitude- and Fluctuation-Based Dispersion Entropy," Entropy-Switz., vol. 20, no. 3, pp. 210, 2018, doi: 10.3390/e20030210.

23. C. Gu, X. Qiao, H. Li and Y. Jin, "Misfire Fault Diagnosis Method for Diesel Engine Based on MEMD and Dispersion Entropy," Shock Vib., vol. 2021, pp. 1-14, 2021, doi: 10.1155/2021/9213697.

24. X. Yan and M. Jia, "Intelligent fault diagnosis of rotating machinery using improved multiscale dispersion entropy and mRMR feature selection," Knowl.-Based Syst., vol. 163, pp. 450-471, 2019, doi: 10.1016/j.knosys.2018.09.004.

25. Y. Ke, C. Yao, E. Song, Q. Dong and L. Yang, "An early fault diagnosis method of common-rail injector based on improved CYCBD and hierarchical fluctuation dispersion entropy," Digit. Signal Process., vol. 114, pp. 103049, 2021, doi: 10.1016/j.dsp.2021.103049.

26. R. Dhandapani, I. Mitiche, S. McMeekin and G. Morison, "A Novel Bearing Faults Detection Method Using Generalised Gaussian Distribution Refined Composite Multiscale Dispersion Entropy," IEEE T. Instrum. Meas., vol. 71, pp. 1-12, 2022, doi: 10.1109/TIM.2022.3187717.

27. Y. Ma, J. Cheng, P. Wang, J. Wang and Y. Yang, "Rotating machinery fault diagnosis based on multivariate

multiscale fuzzy distribution entropy and Fisher score," Measurement, vol. 179, pp. 109495, 2021, doi: 10.1016/j.measurement.2021.109495.

28. Y. Liu, J. Zhang and L. Ma, "A fault diagnosis approach for diesel engines based on self-adaptive WVD, improved FCBF and PECOC-RVM," Neurocomputing, vol. 177, pp. 600-611, 2016, doi: 10.1016/j.neucom.2015.11.074.

29. M. Zhang, Y. Zi, L. Niu, S. Xi and Y. Li, "Intelligent Diagnosis of V-Type Marine Diesel Engines Based on Multifeatures Extracted From Instantaneous Crankshaft Speed," IEEE T. Instrum. Meas., vol. 68, no. 3, pp. 722-740, 2019, doi: 10.1109/TIM.2018.2857018.

30. C. Zhao, J. Sun, S. Lin and Y. Peng, "Rolling mill bearings fault diagnosis based on improved multivariate variational mode decomposition and multivariate composite multiscale weighted permutation entropy," Measurement, vol. 195, pp. 111190, 2022, doi: 10.1016/j.measurement.2022.111190.

31. Y. Ma, J. Cheng, P. Wang, J. Wang and Y. Yang, "Rotating machinery fault diagnosis based on multivariate multiscale fuzzy distribution entropy and Fisher score," Measurement, vol. 179, pp. 109495, 2021, doi: 10.1016/j.measurement.2021.109495.

32. Y. Liu, J. Zhang and L. Ma, "A fault diagnosis approach for diesel engines based on self-adaptive WVD, improved FCBF and PECOC-RVM," Neurocomputing, vol. 177, pp. 600-611, 2016, doi: 10.1016/j.neucom.2015.11.074.

33. B. Mei, L. Sun, G. Shi and X. Liu, "Ship Maneuvering Prediction Using Grey Box Framework via Adaptive RM-SVM with Minor Rudder," Pol. Marit. Res., vol. 26, no. 3, pp. 115-127, 2019, doi: 10.2478/pomr-2019-0052.

34. Y. Ke, C. Yao, E. Song, Q. Dong and L. Yang, "An early fault diagnosis method of common-rail injector based on improved CYCBD and hierarchical fluctuation dispersion entropy," Digit. Signal Process., vol. 114, pp. 103049, 2021, doi: 10.1016/j.dsp.2021.103049.

35. L. Zhang, J. Sun and C. Guo, "A Novel Multi-Objective Discrete Particle Swarm Optimisation with Elitist Perturbation for Reconfiguration of Ship Power System," Pol. Marit. Res., vol. 24, no. s3, pp. 79-85, 2017, doi: 10.1515/pomr-2017-0108.